Available online at www.sciencedirect.com

jmr&t Journal of Materials Research and Technology

journal homepage: www.elsevier.com/locate/jmrt

Original Article

Bentonite as an active natural filler for silicone leading to piezoelectric-like response material

Mihail Iacob [a], *Vasile Tiron* [b,**], *George-Theodor Stiubianu* [a], *Mihaela Dascalu* [a], *Leonor Hernandez* [c], *Cristian-Dragos Varganici* [a], *Codrin Tugui* [a], *Maria Cazacu* [a,*]

[a] *Department of Inorganic Polymers, "Petru Poni" Institute of Macromolecular Chemistry, Aleea Gr. Ghica Voda 41A, 700487, Iasi, Romania*

[b] *Research Center on Advanced Materials and Technologies, Department of Exact and Natural Sciences, Institute of Interdisciplinary Research, Alexandru Ioan Cuza University of Iasi, Bd. Carol I nr. 11, Iasi, 700506, Romania*

[c] *Universitat Jaume I. Departamento de Ingenieria Mecanica y Construccion, Castellon de la Plana, 12071, Spain*

ARTICLE INFO

Article history:
Received 21 June 2021
Accepted 28 December 2021
Available online 31 December 2021

Keywords:
Natural filler
Silicone
Bentonite
Responsive composite
Dielectric permittivity
Functional inorganic material

ABSTRACT

Raw sodium bentonite (Bent) without preliminary treatments is incorporated as a filler in a silicone matrix, from 5 to 100 parts per hundred (pph), by weight, by simple mixing in solution. The mixtures are processed as films and stabilized by condensation crosslinking at room temperature. Besides being environmentally safe and non-toxic, bentonite is 30 times cheaper than polydimethylsiloxane (PDMS), so the cost price of composites can be reduced by over 40%. Studies on the effects of bentonite addition as filler on the properties of composites reveal that thermal stability is not significantly affected, while an increase in the amount of inorganic residue with an increase of Bent content is recorded. More importantly, the mechanical and dielectric properties are significantly influenced by the Bent content in the PDMS matrix. The Young's modulus increases, while the elongation decreases, indicating a stiffening of the material and a decrease in its elasticity as the Bent load increases. Most notably, the dielectric permittivity increases up to more than five times at 10^3 Hz by adding 100 pph Bent, while the dielectric losses remain acceptable, especially at high frequencies for all composites. Furthermore, the study of composite films through Piezoresponse Force Microscopy and piezoelectric testing system reveals an outstanding piezoelectric-like response for composites with a high Bent content. The wide-angle X-ray diffraction indicates an increase of the crystalline fraction - the main factor that influences the apparent piezoelectric coefficient - with increasing the Bent load.

* Corresponding author.
** Corresponding author.
E-mail addresses: vasile.tiron@uaic.ro (V. Tiron), mcazacu@icmpp.ro (M. Cazacu).

https://doi.org/10.1016/j.jmrt.2021.12.125

1. Introduction

A very wide variety of solid materials, organic or inorganic, natural or synthetic, are often used as fillers in polymer processing. Although initially the ingredients (usually cheap) were introduced as extenders to reduce the price of the material, it was quickly realized their ability to change in the desired sense some properties, becoming functional fillers [1–10]. Thus, in addition to cost reduction, the fillers can improve processability or can modify, among others, thermal, mechanical, electrical, magnetic, flame resistance, etc. of the polymers. At the same time, some disadvantages such as fragility or opacity may occur in the resulting materials [10]. The direction and magnitude of these changes depend on the nature and amount of the filler but are also strongly influenced by particles' size, shape and surface chemistry [11]. The use of clay mineral nanofiller montmorillonite (*Mt*) - high aspect ratio octahedral alumina sheets sandwiched between tetrahedral silica sheets - with nylon-6 as coatings for car timing belts initiated by Toyota R&D group in 1991 triggered a new trend in research by preparing clay mineral polymer composites [12,13]. Subsequently, interest in polymer-silicate nanocomposites has rapidly been increasing in industry and in academia, due to their effect of altering many properties, such as absorbance, ion exchange capacity, thermal and solvent resistance, gas barrier properties, flame retardance, mechanical properties (hardness and stiffness) or simply to reduce the cost price [10,14]. Now, polymer-clay mineral composites are of interest for use in constructions, electronics, consumer products and transportation [14], aerospace and biomedical [15]. Many other polymer systems including epoxies, polyurethanes, polyimides, nitrile rubber, polyesters, polypropylene, polystyrene, etc., were used as matrices for clay minerals [16,17]. Among them, polysiloxanes would seem to be an interesting choice as a matrix, given the origin close to that of clay minerals that are aluminosilicates. Due to Si–O bonding inorganic nature, silicone rubber has superior properties to regular organic rubbers in terms of heat resistance, chemical stability, electrically insulating, abrasion resistance, weatherability and ozone resistance [18]. There are already several literature reports on the association of polysiloxanes with clay minerals in nanocomposite materials prepared for certain purposes. Thus, organomodified-nanoclay with negatively charged silicate was incorporated into biomedical grade silicone rubber of interest for tissue engineering. Improving in mechanical properties of the substrate with enhanced strength and stiffness was obtained, while no toxic effects were observed [18]. *Mt* intercalated with heparin - cetyltrimethylammonium bromide complex was incorporated into PDMS to obtain composites that were evaluated for compatibility with blood by hemolysis and platelet adhesion assays [15]. The incorporation of siloxane modified *Mt* into a rapid-cure liquid silicone rubber matrix resulted in materials with reduced water vapour permeability and improved tear strength and compression set values [18].

In the context of our concerns to optimize silicones for use as active elements in electromechanical devices by using various synthetic fillers [19–26], in this paper, a natural one, raw sodium bentonite (Bent), is used as such. A high molecular weight polydimethylsiloxane-α,ω-diol (PDMS) crosslinked at room temperature with tetraethyl orthosilicate (TEOS) is used as matrix. Bent is an ideal material for nano-composites in many industries due to its properties, being used as a plasticizer, binder, thickener, thixotropic agent, suspending agent, filler, decolourizer and can also help to improve the mechanical strength, water-proof, fire-proof and from a biological point of view, it is environmentally safe and non-toxic. The aim of this work is to study the effect of raw sodium Bent loading in atypical amount on some properties (thermal, mechanical, electrical) of the PDMS composites processed as thin films. Coupling between electrical and mechanical phenomena is a common characteristic of many natural systems, like piezoelectric and energy storage materials. Investigation by Piezoelectric Force Microscopy (PFM) and piezoelectric d_{33} testing system of these film-shaped composites revealed piezoelectric-like behavior well-correlated with the Bent content. There are no previous reports in the literature about such composites and approaches from this perspective.

2. Experimental details

2.1. Materials

Polydimethylsiloxane-α,ω-diol (PDMS) with Mn = 230,000 g mol^{-1}, as determined by Gel Permeation Chromatography, was synthesized following the procedure described in the reference [27] through acid catalysed ring-opening polymerization of octamethylcyclotetrasiloxane. Tetraethyl orthosilicate, $Si(OC_2H_5)_4$, with purity >99.0 and dibutyltin dilaurate (DBTDL) were purchased from Sigma–Aldrich, while raw sodium bentonite was purchased from Akoma.

2.2. Preparation of composites films

0.75 g of PDMS was dissolved in 10 ml of toluene, stirred for 24 h at room temperature after which 0.0375, 0.075, 0.15, 0.375 and 0.75 g, representing 5, 10, 20, 50, and 100 pph of commercial Bent were added in order to prepare composites *Cn* (C5, C10, C20, C50, and C100, respectively) and stirred for 60 min. The reference sample was prepared without addition Bent and named C0. Then, 0.07 ml of TEOS and 10 μl of DBTDL were added to the reaction mixture and stirred for another 10 min. Finally, the reaction mixture was poured as thin film on a Teflon substrate and left for crosslinking for 48 h, after which it detashed from the substrate and allowed to mature under laboratory conditions for about two weeks before characterization. In a previous study it was demonstrated that two weeks are enough for full maturation [28].

2.3. Characterization methods

The FT-IR spectra were recorded using a Bruker Vertex 70 spectrometer in transmittance mode (32 scans) on KBr pellet. Hitachi HT 7700 microscope was used to analyse the morphology of Bent (the particles dispersions in toluene were cast on Cu grids (300 mesh) and dried before analysis). The morphology of PDMS-Bent composites was studied using Quanta 200 scanning electron microscope, operating at 20 kV

with secondary and backscattering electrons in low vacuum mode. Identification of the phases in Bent powder was carried out with BRUKER D8 ADVANCE diffractometer with Cu anode (Kα1 = 1.5406) at 25 °C, tension applied to the tube of 40 kV and the intensity of the current of 30 mA. The structure and crystalline order of the PDMS-Bent composite films were analysed by X-ray diffraction (XRD), using a SHIMADZU LabX XRD-6000 diffractometer, with Cu-Kα radiation, in Bragg–Brentano configuration. The powder X-ray diffraction (XRD) patterns of PDMS and PDMS with Bent filler were collected at room temperature in a continuous scanning mode, in the range $2\theta = 5$ - 70°, with a scan rate of 0.25° min^{-1}. The thermal degradation (TG) experiments were performed on a STA 449F1 Jupiter device (Netzsch-Germany). 10 mg of each sample were heated from 30 to 700 °C under a nitrogen flow rate of 50 ml min^{-1} in an open Al_2O_3 crucible with a 10 °C min^{-1} heating rate. Stress–strain measurements were made with an Instron 3365 machine on dumbbell-shaped specimens with a gauge width of 4 mm and a gauge length of 50 mm prepared by die cutting. An extension rate of 200 mm min^{-1} was applied, while for cyclic measurements, the samples were stretched with a speed of 50 mm min^{-1}.

All measurements were made at room temperature. Novocontrol Dielectric Spectrometer Concept 40 was used to measure the complex dielectric permittivity at frequencies between 10^{-1} and 10^6 Hz (room temperature). To perform the measurements, the samples were placed between two golden plated copper electrodes with a diameter of 20 mm. For electrical breakdown measurements, two electrodes based of highly conductive carbon black powder, with a diameter of 10 mm, were concentrically deposited on both sides of the sample. In order to determine the breakdown field, the voltage was increased continuously with a rate of 100 V s^{-1} until the breakdown.

A *piezometer d_{33} testing system*, working in dynamic mode, was used to investigate the direct piezoelectric-like effect and to obtain a quantitative measurement of the piezoelectric-like coefficient. The direct piezoelectric coefficient of the PDMS-Bent composite film samples was determined at room temperature (without poling) using a piezometer (PIEZOTEST PM300 from Piezotest Ltd, London, UK). In order to measure the piezoelectric-like coefficient, each PDMS-Bent composite sample was sandwiched between two copper electrodes. The dynamic d_{33} coefficient was determined by the ratio of the root mean square (RMS) values of generated charge and applied dynamic force (F = 0.25 N).

Piezoresponse Force Microscopy (PFM) was employed to investigate the local electromechanical (piezoelectric-like) properties of the PDMS-Bent composite using a multi-mode AFM setup (NT-MDT Solver Pro). To quantify and to compare the local piezoelectric-like response of the investigated samples, all PFM images were taken during one imaging session using the same cantilever and the same laser position. Commercial probes CSG10 with a platinum conductive coating (NT-MDT), with a radius of curvature R = 35 nm, contact resonance frequency f = 286 kHz and spring constant k = 0.6 N m^{-1} were used in this experiment. PFM images (surface topography, magnitude and phase), with surface scanning area of 20 × 20 μm^2, were obtained in contact mode by applying a loading force of 2.72 nN, drive voltage of 1 V and a scan rate of 0.5 Hz. In this work, the piezoresponse signal was calibrated using both standard calibration procedure (cantilever sensitivity) and test sample (periodically poled $LiNbO_3$) with a known d_{33} piezoelectric coefficient [29].

A detailed description of the PFM technique and the experimental set-up can be found in some reviews [30,31]. Because the piezoelectricity and PFM technique are not as commonly treated and used in polymers testing as in piezoelectric ceramics or inorganic materials, an introductory section about particular aspects in PFM measurements is provided in the following subsection.

2.4. *Particular aspects in PFM measurements*

Based on the atomic force microscopy (AFM), piezoresponse force microscopy (PFM) has become an established, powerful tool for functional nanoscale imaging of electromechanical (EM) active materials [29,32]. Moreover, contact resonance-enhanced method of Piezoresponse Force Microscopy (PFM) has been shown capable of detecting the local surface displacements at picometer level. Commonly, the piezoresponse force microscopy employs electrostriction or converse piezoelectric effect to measure small surface displacements resulting from the application of an external AC electric field between a conducting tip and the sample's surface. The tip follows the expansion and contraction of the surface allowing the voltage-dependent electromechanical (EM) response to be mapped simultaneously with topography using a lock-in technique. The local oscillations of the sample surface are transmitted to the tip and detected by a photodiode, while the signal at the lock-in output is denoted as piezoresponse signal (PRS) [33]. The ratio of tip displacement to applied voltage yields the inverse piezoelectric d_{33} constant. For the piezoelectric materials, the PFM phase and the amplitude images can be interpreted as the direction of polarity and the magnitude of the piezoelectric response along the sample thickness direction, respectively. Although in PFM technique, the EM response is normally due to piezoelectricity, other undesired non-piezoelectric effects, such as electrostatic, ionic, electrostriction, flexoelectricity, interfacial charges accumulation (Maxwell–Wagner), thermal (Joule) effects or synergistic effect, can induce an EM response that resembles the piezoresponse, contributing to the recorded PRS [34,35]. Usually, the quantitative piezoelectric measurements by PFM are doubtful by the difficulty of disentangling, from the total electromechanical response, the contributions of the piezoelectric response and other non-piezoelectric effects. The non-piezoelectric effects can be simultaneously detected as a PFM response and thereby distort the accuracy of PFM measurements. While the mechanism of piezoelectricity in traditional piezoelectric materials relies on ion displacement in the lattice of a non-centrosymmetric system, in non-piezoelectric materials, the mechanisms of EM deformation are essentially different. Hereafter, PRS refers to as the piezoresponse signal recorded by PFM technique (termed as PFM magnitude), which can be generated either by piezoelectric and non-piezoelectric (termed as piezoelectric-like) effects and it is used to estimate the local electromechanical deformation of the sample. The origin and influence of non-piezoelectric effects on PRS are briefly described as follows:

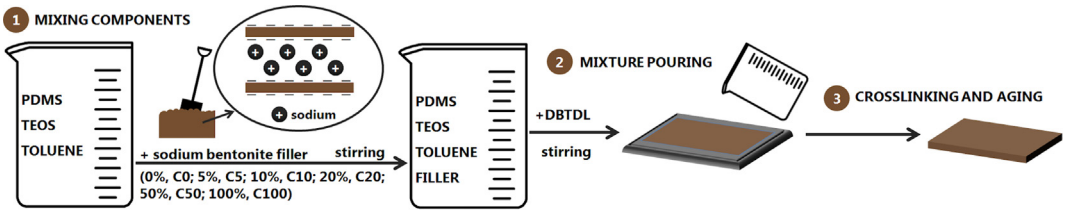

Fig. 1 – Illustration of the preparation procedure of PDMS-Bent composites.

(1) The electrostatic effect originates essentially from the localized electrostatic forces between the tip and sample surface charge and delocalized (long-range) electrostatic forces between the body of the cantilever and the sample surface charge. As the electromechanical response results from the application of a highly localized electric field through a conductive cantilever, the electrostatic forces can cause an additional cantilever deflection, enhancing the PRS. Even though the electrostatic contribution cannot be fully separated from PRS, its contribution can be greatly diminished by using stiffer [29,36], or sharper, or longer tip [37], or higher eigenmodes [38].

(2) A surface displacement induced by ionic phenomena (i.e., ion diffusion and electromigration, and/or electrochemical reactions) is referred to as electrochemical strain. The electrochemical strain takes place, in general, in ionically active materials and can also significantly contribute to PRS, since the external electric field, produced by a voltage applied to the AFM tip, produces a local ion redistribution underneath the AFM tip, which in turn causes local volume change, resulting in a displacement of the sample surface.

(3) The interaction between the charged dipoles in dielectric material and an external electric field results in electrostriction. Under the application of an external electric field, a small shape change can occur in any dielectric material due to electrostriction effect. For a polarization oriented perpendicular to the substrate, a field applied parallel to the charged dipole will result in an EM deformation perpendicular to the substrate, in the thickness direction. Because electrostriction is related with the charged dipoles in dielectric material, its effect becomes significant in soft polymer matrix. The piezoelectric response depends on relative density of the charged dipoles and it is inversely proportional to elastic modulus (Y) of polymer matrix in the thickness direction.

(4) Flexoelectricity is an interaction between the electrical polarization and the mechanical strain gradient (Vegard strain). Because flexoelectricity is related with the strain gradient, its effect becomes more significant in thin films and other nanostructures through the lattice mismatch at the interfaces. Its impact on the observed PFM response may be very small (two orders of magnitude) compared to those of the other contributions (piezoresponse or electrochemical strain).

(5) Thermal (Joule) effect refers to a temperature increase of a sample, when is passed by a current flow, accompanied by a thermal expansion. This effect causes an EM response, which in turn can contribute to the PRS via thermal expansion.

(6) Maxwell–Wagner effect refers to charges accumulation, under high electric field, at heterogeneous interfaces of dielectric materials with different permittivities and conductivities. The accumulated charges at the dielectric interfaces result in an enhancement of the local electric field, which in turn could lead to stronger interaction between the tip and sample surface, contributing to recorded PRS.

In addition, there are others parasitic effects which are detrimental to interpretation and quantification of the local EM deformation and piezoelectric coefficient. These effects include the non-uniform electrical field distribution, mechanical constraints from the immediate (non-activated) surrounding, unknown contact resistance, tip indentation effect, substrate bending effect and system-inherent background contributions.

In order to minimize the contribution of electrostatic effects and parasitic interaction on recorded PRS and to avoid the artifact well known in PFM as “topography cross-talk” or

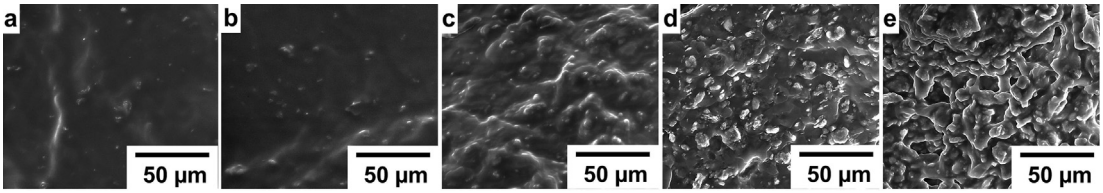

Fig. 2 – Cross-section SEM images of PDMS-Bent composite films.

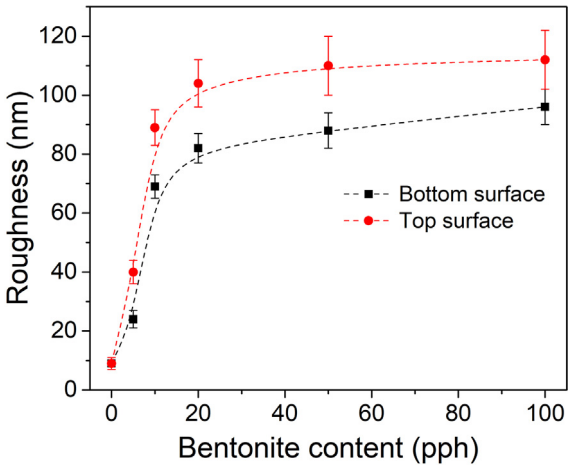

Fig. 3 – Average roughness of top and bottom surfaces of PDMS-Bent composite films.

"electrostatic crosstalk", a complex of preliminary precautions including careful measurement procedures, precise probe calibration, numerous test measurements and special resonance conditions were performed. An extensive description of measurement procedure, calibration procedure and precautions taken during PFM measurements can be found in one of our recent work [39].

3. Results and discussion

3.1. Characterization of raw bentonite

To gain precise information about its composition, structure and morphology, the raw Bent was analysed by Fourier-transform infrared spectroscopy (FTIR), X-ray diffraction (XRD) and transmission electron microscopy (TEM). Common absorption bands for Bent were identified in the FTIR spectrum (Fig. S1): 3638 cm^{-1} (stretching vibrations of OH groups), 1047 cm^{-1} (Si–O bending vibration), 920 cm^{-1} (Al–Al–OH), 525 (Al–O–Si bending vibrations) and 469 cm^{-1} (Si–O–Si bending vibration) [40–42]. The other bands in the spectrum belong to typical compounds found in raw Bent (quartz, calcite, cristobalite, aliphatic hydrocarbons and absorbed water) [41,42]. To identify the crystalline component of raw Bent, wide-angle X-ray diffraction analysis (Fig. S2) was performed. The reflections found in diffractogram of analysed material were assigned to Mt, the main component of raw Bent (ICDD 02–0037) and also the reflections assigned to cristobalite (ICDD 03–0272), quartz (ICDD 47–114) and calcite (ICDD 03–0593). TEM images of bentonite (Fig. S3) show aggregates of layered material, common for Mt and irregularly shaped nanoparticles (quartz, calcite and cristobalite).

3.2. Preparation of PDMS-Bent composites

The sodium bentonite (Bent) powder was gently incorporated by magnetic stirring into the toluene solution of polydimethylsiloxane-α,ω-diol (PDMS) in increasing amounts, 5, 10, 20, 50, and 100 parts per 100 parts weight (php) resulting the composites C5, C10, C20, C50, and C100, respectively. The sample without addition of bentonite was prepared as a reference sample and noted as C0. The composites were processed as thin films with thickness of approximately 0.2 mm, crosslinked through the Si–OH end groups with TEOS in the presence of DBTDL at room temperature and kept in the laboratory environment for about two weeks to allow evaporation of the solvent, complete curing and maturation [28]. The preparation procedure of PDMS-Bent composites is represented graphically in Fig. 1.

3.3. The morphology of the composites

The morphology of composites was evaluated by analysing the cross-section of liquid nitrogen cryo-fractured films by scanning electron microscopy (SEM) (Fig. 2). The reference silicone film (C0) has a smooth aspect without any inhomogeneities. When Bent is incorporated as filler, the surface becomes grained with aggregates evenly dispersed. By increasing the Bent content, the material becomes more and more grained and filler appear as flakes.

The surface roughness of the PDMS-Bent composite films was estimated from AFM images. The influence of the bentonite content on surface roughness is shown in Fig. 3. By increasing the Bent content, the surface roughness gradually increases and tends to saturate for Bent content higher than 20 ppm. The average roughness and its standard deviations are higher for top surface as compared to bottom surface.

3.4. Thermal behaviour of the composites

Thermal characterization of the composite materials was undertaken by the TG analysis. The data extracted from the TG curves (Fig. 4a) are given in Table 1. It can be seen that all composites follow a three-stage thermal decomposition pattern. These steps are more obvious as the addition of Bent is increased. The first stage ranges from 32 °C to 106 °C with a maximum mass loss of 3.21 wt% (Table 1) and corresponds to physical dehydration. The second thermal decomposition stage occurs in the range 193 °C – 403 °C with the highest mass loss of 18.05 wt% for sample C100, and the lowest value, of 3.07%, for sample C20. The next highest mass loss on the second stage of thermal degradation (17.43%) was recorded for the reference sample, C0.

According to *Thomas and Kendrick* [43,44], this is the thermal decomposition initiation stage, occurring through random intermolecular or intramolecular redistribution reactions taking place between siloxane bonds in the matrix and proceeding with the formation of intermediate transition states with the yielding of volatile siloxane cyclic entities. The authors stated that the crosslinked nature of the matrix induces decreased chains flexibility compared to the linear polymer, thus explaining the lower generated mass loss value during this thermal degradation stage and the highest mass loss in the third stage.

According to these aspects, the polymer matrix generates small quantities of cyclic oligomer siloxane entities and higher ones of linear siloxane moieties (i.e. dimers, trimers

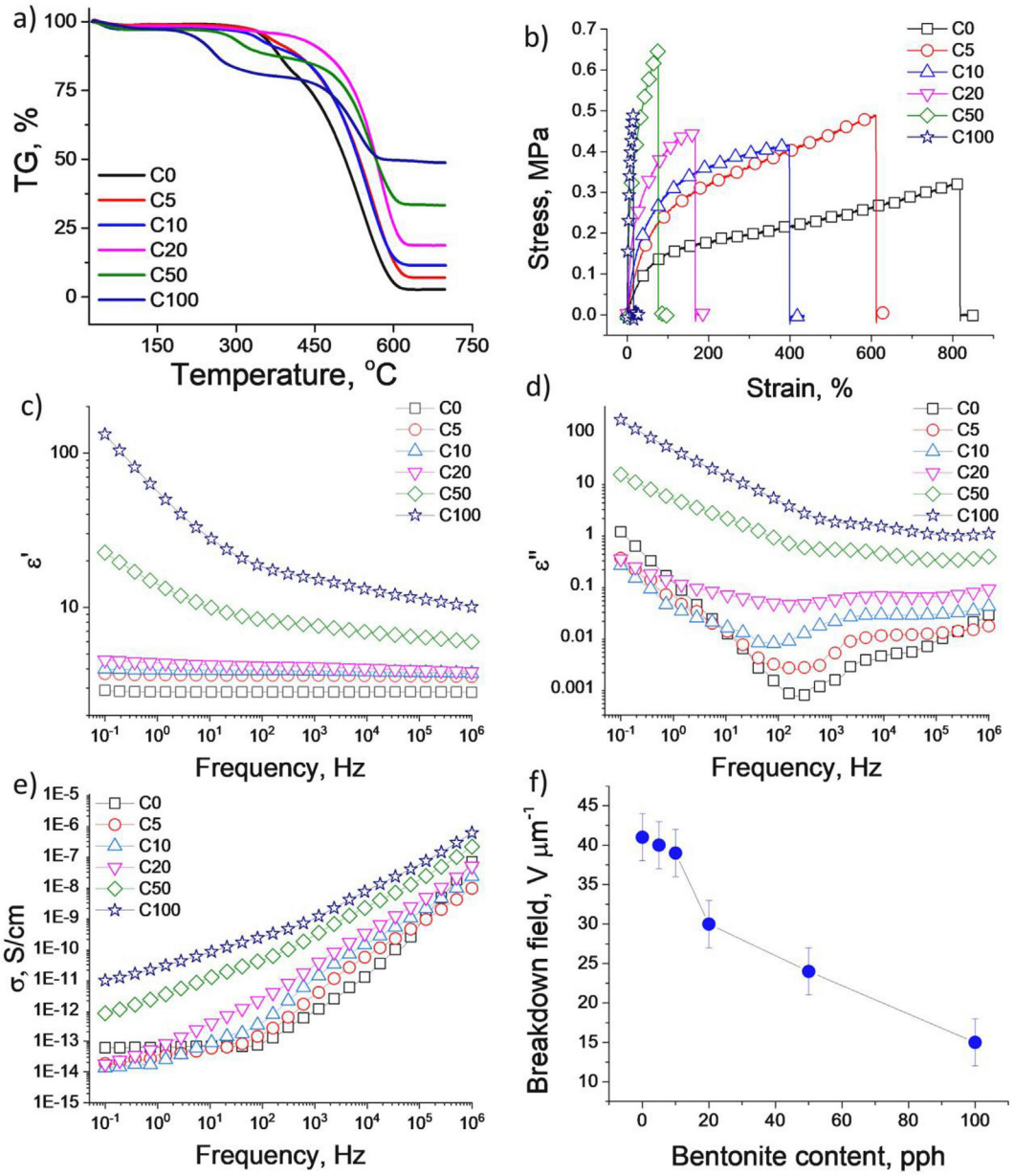

Fig. 4 – TG curves (a); stress–strain curves (b); frequency variation curves of: dielectric permittivity (c), dielectric loss (d), and conductivity (e); dielectric breakdown (f) in dependence on the bentonite load of PDMS-Bent composites.

and others), all thermally decomposing in the last stage through complex overlapping processes, resulting in considerable higher mass losses. By analysing Fig. 4a and Table 1, it may be seen that the thermal stability of the composites increases in the order C100 < C50 < C10 < C0 < C5 < C20. Furthermore, the initiation of thermal degradation takes place with only 3.07% mass loss for composite C20 and 7% and 7.56% mass losses for composites C5 and C10, the latter's thermal stability (T_{onset} = 320 °C) being just slightly lower than that of the polymer matrix C0 (T_{onset} = 325 °C).

These mass loss values of samples C20, C5 and C10 are considerably lower than that of the initial polymer matrix C0 (17.43%) and the rest of the structures (Table 1). By comparison to the reference sample C0, it is clear that the composites exhibit superior thermal stability up to Bent concentration of 20%. The third thermal decomposition stage, where the highest mass loss occurs, ranges between 407 °C and 616 °C and with a mass loss between 30.21% and 84.05%. The percentage of residue remaining at the end of the thermal degradation process (W_{rez}) increases with Bent concentration from 2.54%, for sample C0, to 48.64%, for sample C100.

3.5. *Mechanical properties of the composites*

The mechanical properties of PDMS-Bent composites were evaluated by uniaxial tensile tests and the obtained results are presented in Fig. 4b and Table 2. The stress–strain curves reveal that the addition of Bent within the silicone matrix determines a sharply decrease of the breaking strain, from around 800% recorded for sample C0 (with no filler) to 15% for

Table 1 – The main thermal data extracted from TG curves.

Sample	Stage	T_{onset} (°C)	T_{max} (°C)	T_{endset} (°C)	W_m (%)	W_{rez} (%)
C0	I	34	38	62	1.83	2.54
	II	325	365	385	17.43	
	III	421	540	605	78.15	
C5	I	32	37	79	2.00	6.73
	II	330	381	401	7.00	
	III	407	563	616	84.05	
C10	I	36	40	69	2.84	11.34
	II	320	345	369	7.56	
	III	420	556	608	77.97	
C20	I	38	42	82	2.20	19.06
	II	332	384	403	3.07	
	III	427	573	614	75.57	
C50	I	39	38	90	3.21	33.13
	II	260	299	334	10.71	
	III	462	555	612	52.49	
C100	I	32	52	106	2.80	48.64
	II	193	257	287	18.05	
	III	438	529	563	30.21	

T_{onset} - the onset thermal degradation temperature.
T_{max} - the temperature that corresponds to the maximum rate of decomposition for each stage evaluated from the peaks of the first derivative (DTG) curves.
T_{endset} - the endset thermal degradation temperature.
W_m - the mass loss rate corresponding to T_{max} values.
W_{rez} - the percent of residue remaining at the end of thermal degradation (700 °C).

sample C100 (with 100 pph of bentonite). Also, the increasing amount of bentonite from the PDMS-Bent composite determines a systematic increase of Young's modulus. For example, the sample C0 shows a Young's modulus of 0.27 MPa, while by adding 5 pph of filler increases to 0.48 MPa (sample C5), 10 pph to 0.65 MPa (sample C10), 20 pph to 0.97 MPa (sample C20), 50 pph to 2.85 MPa (sample C50) and, by adding 100 pph of bentonite increases to 4.41 MPa. Ignoring the Mullins effect that occurs at first cycle, all samples show a relatively low mechanical hysteresis (Fig. S4), which increases with the amount of filler incorporated into the polymer matrix (Table 2).

3.6. *Dielectric properties of the composites*

The dielectric properties of the PDMS-Bent composites were measured as a function of frequency at room temperature (Fig. 4c). The dielectric permittivity, dielectric losses and conductivity values at 10^{-1} and 10^{3} Hz are presented in Table 3.

As expected, the ε' increases with increasing the Bent content in the composites. At 10^{-1} Hz, a moderate increase is observed when using up 20 pph of Bent (C20), when it was registered a $\varepsilon' = 4.6$ compared to $\varepsilon' = 2.9$ for pure PDMS. The use of the larger quantity of Bent in the composites has led to a significant increase of ε', being 22.6 for composite with 50 pph filler (C50) and 132.3 for 100 pph. However, with this great increase of the dielectric permittivity, the dielectric loss has also increased as follows: $\varepsilon'' = 14.3$ for C50 and $\varepsilon'' = 165.9$ for C100. A similar trend was observed at higher frequencies. The dielectric permittivity was increased at 10^{3} Hz, from 2.8 for pure PDMS up to 15.2 for C100. At this frequency, the dielectric loss remains at a low value (<1) for all samples excepting sample C100 where $\varepsilon'' = 1.7$. A sharp increase in permittivity at low frequencies seen in the case of sample C100 can be attributed to the electrode polarization phenomenon and indicates mobile charged species in the material [45]. However, the very low values of conductivity highlighted that all samples are electrical insulator materials.

Table 2 – The main mechanical properties estimated on the basis of stress–strain curves.

Sample	Strain at break, ε, %	Stress at break, σ, MPa	Young Modulus[a], E, MPa	Mechanical hysteresis[b], J cm^{-3}
C0	817	0.32	0.27	$6.75 \cdot 10^{-3}$
C5	611	0.48	0.48	$11.39 \cdot 10^{-3}$
C10	396	0.41	0.65	$18.93 \cdot 10^{-3}$
C20	165	0.44	0.97	$30.19 \cdot 10^{-3}$
C50	75	0.65	2.86	n/a
C100	15	0.49	4.41	n/a

[a] Determined from the slope of stress–strain curves using a linear fit.
[b] Determined graphically by calculating the area between the second loading–unloading cycle.

Table 3 – Dielectric properties of PDMS-Bent composites.

Sample	Dielectric permittivity, ε′		Dielectric loss, ε″		Conductivity, S- cm^{-1}	
	0.1 Hz	10^3 Hz	0.1 Hz	10^3 Hz	0.1 Hz	10^3 Hz
C0	2.9	2.8	1.1	$2.3\cdot10^{-3}$	$6.1\cdot10^{-14}$	$1.5\cdot10^{-12}$
C5	3.7	3.6	0.3	$4.8\cdot10^{-3}$	$1.8\cdot10^{-14}$	$3.2\cdot10^{-12}$
C10	4.0	3.9	0.2	$1.9\cdot10^{-2}$	$1.4\cdot10^{-14}$	$1.3\cdot10^{-11}$
C20	4.6	4.1	0.3	$5.3\cdot10^{-2}$	$1.8\cdot10^{-14}$	$3.6\cdot10^{-11}$
C50	22.6	7.6	14.3	$4.9\cdot10^{-1}$	$8.0\cdot10^{-13}$	$3.3\cdot10^{-10}$
C100	132.3	15.2	165.9	1.7	$9.2\cdot10^{-13}$	$1.1\cdot10^{-9}$

Beside mechanical and dielectric properties, the prepared PDMS-Bent composites were evaluated by measuring the electrical breakdown field (E_b) and the obtained data are presented in Fig. 4d. The breakdown measurements were conducted by applying a ramp signal with a slope of 100 V s^{-1}, similarly to procedure described in reference [46]. The voltage was stepwise increased until the breakdown occurs. The electrical breakdown field decreases with the increasing concentration of bentonite. However, at low concentrations up to 10 pph (E_b(C5) = 40 V μm^{-1} and E_b(C10) = 39 V μm^{-1}), the breakdown values are almost identical with those measured on sample C0 (E_b(C0) = 41 V μm^{-1}). By increasing the bentonite concentration, the electrical breakdown decreases to E_b(C20) = 30 V μm^{-1}, E_b(C50) = 24 V μm^{-1} and E_b(C100) = 15 V μm^{-1}, respectively.

3.7. *Piezoelectric-like behaviour investigation*

As previously shown, Bent was originally chosen as a filler for cost effective in preparation and environmental reasons, as it is a material that is found in abundance in nature and is non-toxic. It has been found that the incorporation of Bent in polymer matrix acts as a dielectric permeability enhancer without significantly compromising mechanical properties of composite (material remains flexible and mechanically stretchable). In a previous work, *Song* has found that Bent addition to PVDF polymer increases the piezoelectricity performance (d_{33}) of the latter, *e.g.* by 31.3% at a 2 wt% filler load [47]. Since the PVDF is a piezoelectric polymer, more precisely, ferroelectric, while Bent itself is considered a non-piezoelectric material, it was expected that the enhanced piezoelectricity to be attributed to the promotion of the formation of the crystalline β phase in the polymer matrix. It is well known that, from all five crystalline phases (α, β, γ, δ and ε) of PVDF polymer, the β-phase presents the highest dipole moments, resulting in a high spontaneous polarization and therefore enhanced piezoelectric performance [48]. *Song* found that piezoelectric coefficient d_{33} increased, while the volume fraction of β phase in the samples ($v\beta$) is reduced by the fillers load, so he concluded that d_{33} of the composites does not depend totally on their $v\beta$ and other factors need to be taken into account. As less β phase was formed in composite, it was concluded that combined piezoelectricity from Bent filler and β phase of PVDF might be responsible for the enhancement of piezoelectric coefficient [47]. Since the Bent itself is a non-piezoelectric material, other non-piezoelectric effects may contribute to the enhancement of piezoelectric-like coefficient of PVDF with Bent filler.

3.7.1. *Piezometer measurements*

In the present paper, our purpose was to see if such an effect is manifested when bentonite is incorporated into an amorphous polymer such as polydimethylsiloxane. First, the composite films were investigated using a piezometer testing system, commonly used to highlight the piezoelectric behaviour and to quantify the direct piezoelectric constant. Experimental data of direct piezoelectric coefficients of the samples containing different percentages of Bent clearly show that the dynamic piezoelectric-like coefficient increases with increasing the filler content in the composite. Thus, by increasing the bentonite load from 5 pph to 100 pph, the piezoelectric-like coefficient increases from 5 pC N^{-1} to 35 pC N^{-1}. The influence of Bent concentration on the direct piezoelectric-like coefficient can be seen in Fig. 5.

Although, the piezometer testing system offers information on the average value of the apparent piezoelectric coefficient of bulk material, more valuable information can be obtained from PFM measurements. Beside average value of the apparent piezoelectric coefficient, PFM technique allows local surface displacement to be mapped simultaneously with topography.

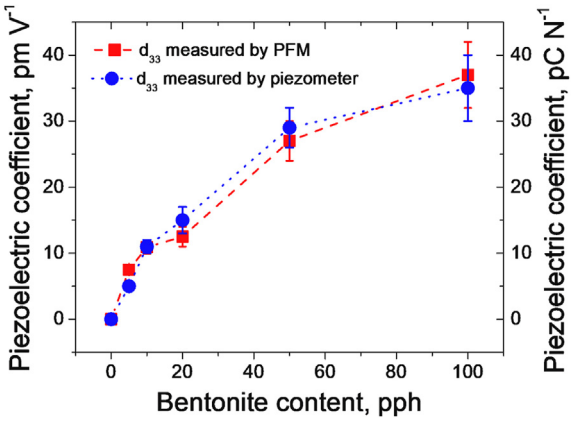

Fig. 5 – The dependence of apparent piezoelectric coefficient on the percentages of Bent in composite films measured with piezometer (blue points) and by piezoresponse force microscope (PFM). Dashed lines are meant to guide the eye.

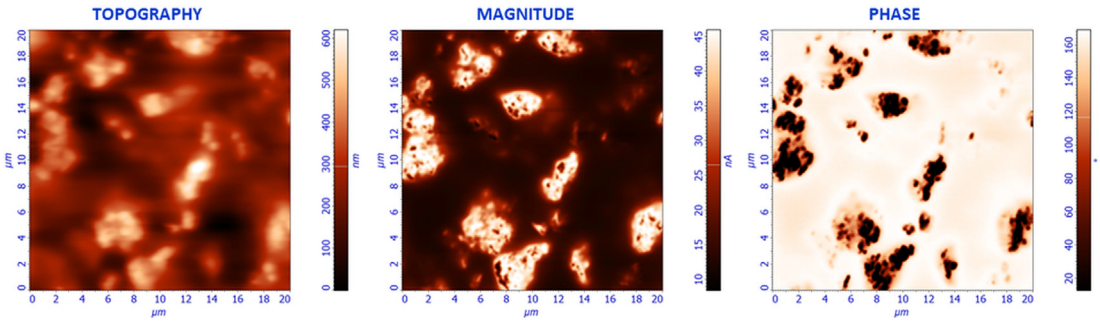

Fig. 6 – Piezoelectric force microscopy images of unpoled PDMS-Bent composite with 100 pph (C100) of Bent obtained at a drive voltage of 1 V and scan rate of 0.5 Hz.

3.7.2. *PFM measurements*

The piezoelectric-like effect of PDMS-Bent composites containing different percentages of Bent (5, 10, 20, 50 and 100 pph) was measured using contact resonance-enhanced methods of Piezoresponse Force Microscopy (PFM). Out-of-plane PFM signals were acquired on bottom side of the sample to get insight into the local EM deformation of PDMS film with Bent filler. Typical PFM images consisting of surface topography, magnitude and phase are presented in Fig. 6 and S5 for samples with Bent content of 100 pph. A lot of irregularly-shaped regions can be observed in all PFM images. This demonstrates that Bent nanoparticles agglomerate and these assemblies are widespread in the composite film. In both cases, the magnitude and phase images show a variety of contrasts implying widespread of local "*piezoresponse*" and allow identifying areas with enhanced EM response. The features seen in magnitude image are comparable to those seen in topography image and this could be likened to a crosstalk between topography and PFM response. But, in this work, in order to avoid the topographical crosstalk, the images were acquired with a very low scanning speed (10 μm s^{-1}, corresponding to scanning rate of 2 s/line) by resonance-enhancement PFM measurements.

As previously shown, the "*piezoresponse*" mainly comes from Bent filler and it is expected that the Bent nanoparticle conglomerates to exhibit highest PRS. It should be mentioned that under the same PFM measurement conditions, a PDMS reference gave practically no similar response.

During PFM measurements, in ideal conditions, the piezoresponse of the sample is either in phase, or out of phase with the applied alternating voltage. This means that the measured PFM phase can only have two values, whose difference is 180°. But, due to electrostatic force, cantilever dynamics, intrinsic material properties, tip-sample contact, instrumental offsets including phase delays in cables and analog signal processing, this requirement is rarely fulfilled. From all above-mentioned effects, the electrostatic force seems to have the most detrimental effect on the phase image, diminishing the phase difference between antiparallel domains [37]. However, in our case, the phase difference is nearly 180°, which means that the electrostatic contribution was suppressed and the PFM magnitude image can be used to quantify the surface local displacement.

Since the Bent filler showed piezoelectric-like effect under mechanical deformation, an effective piezoelectric coefficient can be defined. For a piezoelectric material, the effective piezoelectric coefficient d_z can be expressed as $d_z = 2Q_zP_ze_0e_z$, where Q_z is the longitudinal electrostriction coefficient, P_z is the spontaneous polarization vector component along the laboratory coordinate z (normal to sample's surface), e_o and e_z are the dielectric permittivity of vacuum and material, respectively. The quantification of PFM amplitude (*piezoresponse*), i.e., the conversion of PFM magnitude signal from *nA* to *pm* V^{-1}, is commonly performed using the cantilever static deflection sensitivity, which is extracted from static force–distance curves [49].

Fig. 7 shows the distribution on PFM amplitude, extracted from PFM magnitude image (Fig. 6) after quantification with cantilever sensitivity. The mean value of apparent piezoelectric coefficient estimated from the histogram of PFM amplitude (Fig. 7) is 22.4 pm V^{-1}. However, as the PFM magnitude image was aquired using the traditional optical beam detection method, the measurements accuracy of piezoelectric-like coefficient may be distort by the cantilever beam dynamics

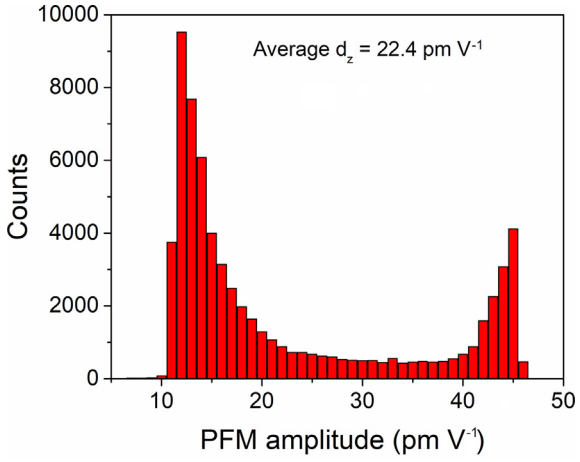

Fig. 7 – PFM amplitude distribution of C100 sample, extracted from PFM magnitude image after quantification with cantilever sensitivity.

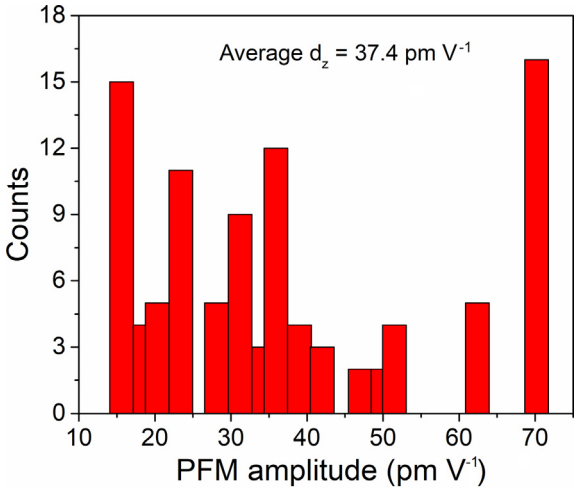

Fig. 8 – PFM amplitude distribution of C100 sample, extracted from magnitude-bias curves after quantification with cantilever sensitivity.

[50]. We should bear in mind that during PFM scan, an optical beam deflection is used to track the cantilever deflection change, a deflection which is also sensitive to the local slope of the cantilever, not only to the z-shift of the probe tip. When the PFM scan is performed on near contact resonance, the behavior (deflection) of the cantilever beam during the vibrations is greatly dependent on cantilever geometry and stiffness and probe-sample contact area and adhesion force. Therefore, the cantilever beam dynamics during PFM scan may be an important source of artifacts as topography crosstalk and electrostatic force that drive the cantilever beam motion. Moreover, the behavior of the cantilever beam during the scan is different from the behavior acquired during calibration of the probe sensitivity with static force–distance curves. Since the PFM amplitude was obtained from PFM magnitude images after quantification with static cantilever sensitivity, the quantitative assessment of the piezoelectric-like coefficient may be hampered by the cantilever beam dynamics effect.

The effect of cantilever beam dynamics can be removed by measuring the local piezoelectric effect at single point on the sample. The PFM system used in this work (Solver Pro from ND-MDT) allows to probe the local piezoresponse of the sample by recording magnitude – bias voltage curves in a single point on the sample. The magnitude - bias voltage curves are typically measured by ramping a DC voltage applied between tip and sample and recording the piezoresponse (PFM magnitude signal). The local apparent piezoelectric coefficient values (since the PRS is caused by a non-piezoelectric effect) were estimated from the piezoresponse curves using static cantilever sensitivity. For each PDMS sample with different percentages of Bent, the mean value of piezoelectric-like coefficient was calculated by averaging piezoresponse measurements performed within a specific grid (10 × 10 points matrix) on a surface area of 20 × 20 μm^2. Fig. 8 shows the PFM amplitude distribution recorded on C100 sample, extracted from magnitude-bias curves after quantification with cantilever sensitivity. The scatter of the piezoresponse amplitude values is relatively high due to the softness and intense inhomogeneity of the sample (see Fig. 6). The local PFM amplitudes fluctuate between 15 and 70 pm V^{-1}, but even higher values (110 pm V^{-1}) were recorded on different investigated area on the sample. The average value of apparent piezoelectric coefficient estimated from the histogram of PFM amplitude (Fig. 8) is 37.4 pm V^{-1}.

In addition, the piezoresponse of the C100 sample was triple checked by PFM technique by performing surface displacement procedure (Fig. S6) [36]. In this aim, a pair of copper electrodes was deposited on both sides of the sample. The top electrode was biased by applying an AC voltage with peak-to-peak amplitude of 10 V and frequency of several Hz, while the bottom electrode was grounded. The surface displacement was monitored by recording the deflection of the laser beam from unbiased cantilever in contact with the top electrode surface. Using this procedure, the electrostatic interaction between the tip and sample's surface is minimized because conducting tip is held at the same potential as the top electrode, and thus, the potentially large source of errors, as topography crasstalk and electrostatic forces, is eliminated. The surface displacement signal recorded by photodetector, which has *nA* unit, was converted in real displacement (*pm* unit) by multiplying the static cantilever sensitivity. The value of piezoelectric-like coefficient estimated from this measurement procedure was 35 pm V^{-1}, a value which is similar to that estimated by piezometer and very close to that estimated from PFM measurement using magnitude-bias voltage curves (37.4 pm V^{-1}).

Based on results reported above, the PFM magnitude-bias voltage curves measurement procedure was further used to estimate the average values of apparent piezoelectric coefficient of PDMS-Bent composite samples containing different amounts of filler. The results plotted in Fig. 5 shows that the average value of the apparent piezoelectric coefficient increases with increasing percentage, by weight, of Bent. The PDMS-Bent composite film with 100 pph Bent shows the best piezoresponse, with an average value of 37 pm V^{-1}. The apparent piezoelectric coefficient of PDMS-Bent composites is comparable to that of the traditional piezoelectric ceramics and ferroelectric polymers [51]. As can be seen, the Bent content has a strong influence on the local piezoelectric-like response of PDMS-Bent composite film, the average values of piezoelectric-like coefficient gradually increase, from 7.5 to 37 pm V^{-1}, as Bent percentages increase from 5 to 100 pph. It should be noted that the PFM measurements performed onto top side of the samples reveal almost the same average values for average piezoelectric-like coefficient, but with higher standard deviations. The direct d_{33} piezoelectric-like coefficient values determined by piezometer are in good agreement with those values measured by PFM technique. Thus, the direct piezoelectric coefficient measured by piezometer testing system proves the accuracy and truthfulness of quantitative measurement of the apparent piezoelectric coefficient by PFM technique. Since the PDMS is completely nonpolar, amorphous, dielectric and non-piezoelectric polymer, while the Bent itself is considered a non-piezoelectric material, the origin of piezoelectric-like behavior in PDMS-Bent composite must be elucidated. In

addition, the absence of resonance peak in the dielectric function proves that PDMS-Bent composite polymer is not a piezoelectric material [52].

3.8. *Origin of piezoelectric-like response in PDMS-Bent composites*

Raw bentonite has a complex composition, it being mainly formed of *Mt* and free minerals, such as quartz, calcite, cristobalite, aliphatic hydrocarbons and absorbed water. Montmorillonites consist of high aspect ratio octahedral alumina sheets sandwiched between tetrahedral silica sheets, designated as tetrahedral - octahedral - tetrahedral (TOT) layers. In reality, the tetrahedral and octahedral alumina sheets are slightly distorted, meaning that a small fraction of the tetrahedral Si atoms is isomorphically substituted by Al and/or a fraction of the octahedral atoms (Al) is substituted by atoms of lower oxidation number. The resulting charge deficiency is balanced by cations, mainly Na, which more than 80% are located between the parallel TOT clay layers. In nature, bentonites usually are formed in aqueous environments having a water content of 15–35%. Consequently, the cations are partially hydrated and only slightly held by the negatively charged clay layers. The negatively charged TOT layers are packed one above the other and the charge compensating cations are located between the layers forming electric double layers [50]. The montmorillonites are capable of quasi-permanently storing electric charges at their surface or in bulk. Having a quasi-permanently electric charges, the *Mt* incorporated into silicon matrix behaves like electrets and may exhibit apparent piezoelectricity. Since the Bent has a lamellar/sandwich structure with high aspect ratio, the piezoelectric-like behaviour comes from the excess of charges stored on the internal surface of TOT layers. The electret properties of the Bent originate from the space-charges stored in the Bent bulk and from surface-charge layers. The Bent filler containing surplus charges can be regarded as heterogeneous inclusions immersed in nonpolar and non-piezoelectric PDMS polymer matrix. In fact, the Bent electrets are solid dielectric materials with a quasi-permanent electric moment, which can exhibit a static electric field, even in the absence of an applied external electric field. *Belhora* et al. [53] have demonstrated that the induced static electric field by electrets allows the electrostrictive polymer to work in a pseudo-piezoelectric mode. Under external electric field, the electrostriction is caused by the displacement of ions in the crystal lattice in the direction of the applied electric field. This displacement will accumulate throughout the bulk material and result in an overall strain (elongation) along the thickness direction. *Vice versa*, when the material is mechanically stressed and deformed, there is a change in the distribution of ions in crystal lattice accompanied by a flow of charge from one electrode to the other. In our case, under the application of mechanical stress, the space between the electrets is compressed and the total interaction between the Bent charged particles should involve both short-range repulsion forces, due to partially bound hydrated cations located between the parallel TOT clay layers and a longer-range repulsion due to ions surrounding charged particles [54]. Therefore, pseudo-piezoelectricity in Bent electrets may result from the deformation of the space-charge volume and from interaction of surface-charge layers. To find the origin of piezoelectric-like behaviour in PDMS-Bent composite polymer, the influence of AC excitation frequency on local piezoresponse was investigated. During PFM measurements, the local piezoresponse (PFM magnitude signal) and vibration amplitude of the samples were measured by recording magnitude – bias voltage curves in a single point on the sample. The magnitude - bias voltage curves are measured by ramping a DC voltage applied between tip, which is also excited by AC voltage with a typical frequency (first harmonic), and the sample. Fig. 9a shows the influence of excitation frequency on the surface displacement of sample C50. The film was excited with AC voltage of 1 V and frequencies $f = 54.2$ kHz (first harmonic) and $f = 108.4$ kHz (second harmonic), while DC voltage was swept from 0 to 10 V. For the second harmonic excitation the amplitude of surface displacement is four times lower as compared to amplitude of surface displacement recorded during first harmonic excitation. The average value of apparent piezoelectric coefficient decreases from 26.5 ± 0.5 pm V^{-1} to 6.5 ± 0.1 pm V^{-1} as the excitation frequency was switched from first to second harmonic. The quadratic dependence of the vibration amplitudes *versus* the excitation frequency was reported for cellular electret polymer by Hillenbrand et al. [55]. In addition, using first harmonic excitation, but decreasing the excitation AC voltage, from 1 V to 0.5 V, a quadratic dependence of the vibration amplitudes *versus* the excitation AC voltage was obtained (Fig. 9b). This indicates a quadratic coupling between the strain and the polarization, a typical dependence for electrostriction effect [35].

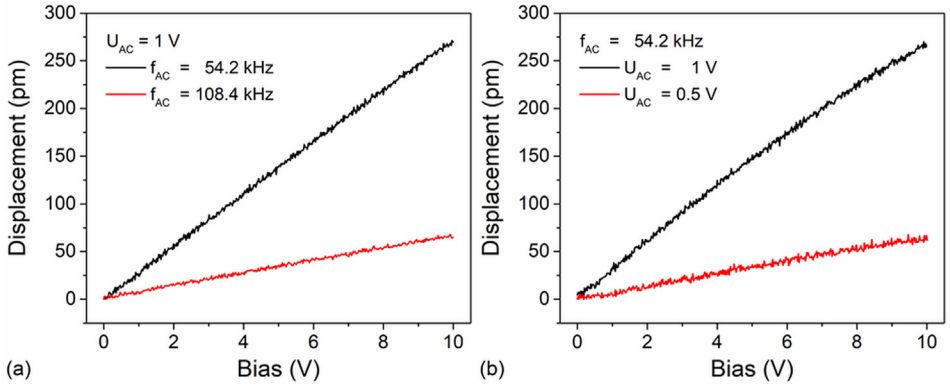

Fig. 9 – The influence of excitation frequency (a) and AC voltage (b) on the surface displacement of sample C50.

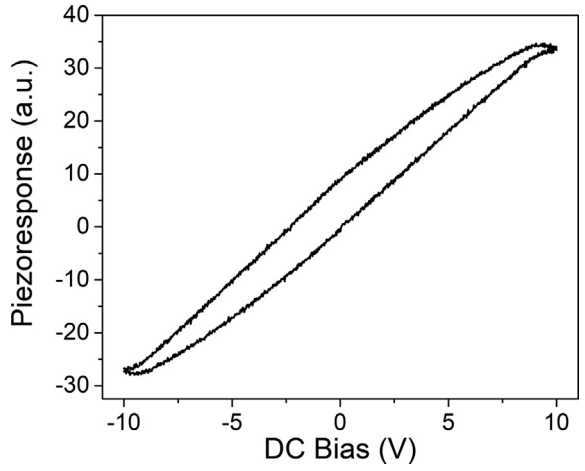

Fig. 10 – Local PFM hysteresis loop (piezoresponse *versus* DC bias voltage) measured on C50 sample.

3.9. *Influence of Bent content on piezoelectric-like behaviour*

In fact, it was shown that the macroscopic piezoelectric-like behaviour depends strongly on Bent concentration, which, in turn, is linked to the relative density of quasi-permanently electric charges stored in Mt. Beside Bent concentration, the piezoelectric-like behaviour depends on the shape anisotropy of Bent particles and mechanical anisotropy of the PDMS-Bent composite. Since the fillers' shape appear as flakes, having a high aspect ratio and a lamellar/sandwich structure (Fig. S3), in polymer matrix they are mainly stacked one above the other (see Fig. 2) with TOT layers perpendicular to the sample's thickness direction, enhancing the quality of the crystallite alignment and leading to formation of a stable oriented (self-polarized) structure. In addition, the static electric field of each particle can favor this orientation. This means that space-charge and surface-charge layers have a preferential orientation (in the film plane) and an external electric field applied normal to the film's surface will result in a surface displacement. Usually, for an electrostrictive (non-piezoelectric) polymer, it is necessary to induce a polarization with a DC bias to obtain a pseudo-piezoelectric behaviour. In PDMS-Bent polymer composite case, the large shape anisotropy (plane-parallel geometry) and packing mode (preferential orientation) of Bent filler result in a remanent polarization and large piezoelectric-like response without poling. The remanent polarization in the PDMS-Bent polymer composite is highlighted by hysteresis measurements of piezoresponse *versus* DC bias voltage. Fig. 10 shows the local PFM hysteresis loop measured on C50 sample. The DC bias voltage was swept from −10 to +10 V, while the excitation AC signal was set to 1 V amplitude and 54.2 kHz frequency. The local hysteresis measured on C50 sample tends to saturate within the bias range ±10 V, and shows a narrow loop.

The electrostrictive effect is due to the electrostatic forces, which increase with dipole density, and therefore should be independent of the electret charges (poling polarity). The phase and the amplitude in the piezoresponse can be interpreted as the direction and the magnitude of the surface displacement, respectively. In this work, by increasing the amplitude of bias voltage, the magnitude of the piezoresponse increases regardless of poling polarity (Fig. S7), whereas the sign of the phase is dependent on the polarity of the classical piezoelectric materials. In addition, experimental results reveal that after poling, at room temperature, the piezoelectric-like coefficient d_z of C100 sample increases up to 55.6 pm V^{-1} (by 50%), demonstrating electromechanical response comparable to the best ferroelectric polymers [56]. Typical PFM images of poled C100 sample can be found in Supporting Information (Fig. S5). In addition, the intrinsic structure (plane-parallel geometry) and preferential orientation (in film's plane) of Bent particles result in a mechanical anisotropy in the PDMS-Bent composite, a necessary condition for the occurrence of piezoelectric-like effect.

Fig. 10 shows a small remnant polarization, highlighting however the presence of an internal electric field. It is possible that DC bias applied during PFM measurement to induce a static electric field, allowing even more the PDMS-Bent composite polymer to work in a pseudo-piezoelectric mode. In addition, the induced electric field could lead to an interfacial charges accumulation into the PDMS-Bent composite polymer, a behavior which is described by the Maxwell–Wagner effect [57]. According to this, the density of the accumulated charges at the heterogeneous interface is determined by the conductivity and permittivity of the component materials [58]. In this work, both conductivity and permittivity of the PDMS-Bent composite increases with the Bent content, pointing out that Maxwell–Wagner effect could also contribute to the piezoresponse-like signal measured by PFM. Moreover, the Maxwell stress also shows a quadratic coupling between the strain and the polarization [59], just like in the case of electrostriction effect.

Therefore, from all non-piezoelectric effects (electrostatic, electrochemical strain, electrostriction, flexoelectricity, thermal and Maxwell–Wagner) presented above, the synergistic effect between Maxwell stress and electrostriction effect seems to be the most likely to contribute to the recorded

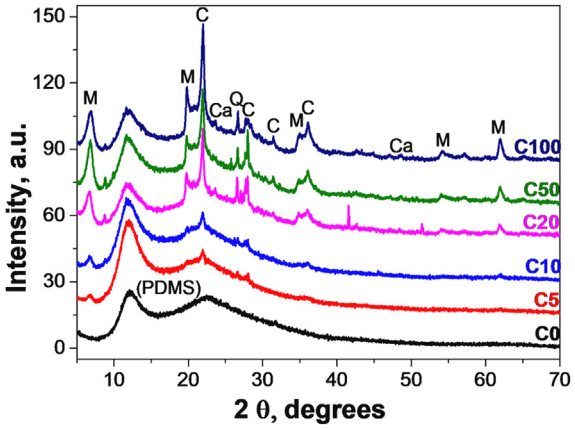

Fig. 11 – XRD patterns of PDMS-Bent composite films with different bentonite loads (pph).

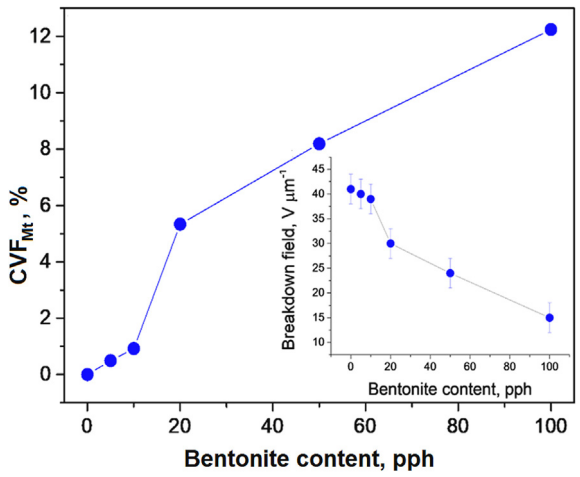

Fig. 12 – Crystalline volume fraction of *Mt* (CVF_{Mt}) in PDMS-Bent composites containing different percentages of bentonite. Inset: breakdown field as a function of bentonite content – the variation is mirror image of CVF_{Mt}.

piezoresponse-like signal in PDMS-Bent composite. However, the quantification and the contribution of each effect on PRS signal are difficult to obtain due to a lack of effective experimental means, like thermally stimulated discharge (TDS) [60] and pulsed electro-acoustic (PEA) [58] techniques.

The PDMS-Bent electrets composite can be modeled as a physical system consisting of positively and negatively charged layers, coupled by two types of springs representing the mechanical properties of two phases, one corresponding to the polymeric matrix (PDMS), and the other, to the TOT structure (bentonite). The bentonite can be modeled as a sandwich made of elastic layers (positive space-charge) interposed between rigid layers (negative surface-charge layers). Since the elastic modulus of the two phases are much different (0.27 MPa for PDMS and 300 MPa for Bent) and Bent filler has a high aspect ratio and a preferential packing mode (orientation), a certain mechanical anisotropy may appear in the PDMS-Bent composite.

Fig. 5 clearly shows that the d_{33} coefficient depends on Bent concentration in the *Cn* composite. As the excess charges are stored on the internal surface of tetrahedral - octahedral - tetrahedral (TOT) clay layers of *Mt*, the apparent d_{33} coefficient should be well related to the amount of *Mt* crystalline phase in the composite.

The obtained XRD patterns (Fig. 11) show the presence of both amorphous PDMS and polycrystalline Bent phases in the composite. As expected, the crystalline order of composite films gradually increases as Bent percentage increases. The crystalline volume fraction of *Mt*, CVF_{Mt}, has been calculated according to [61]:

$$CVF_{Mt} = I_{Mt\_crys} / (I_{B\_crys} + I_{am}) \quad (1)$$

where, I_{Mt_crys}, I_{B_crys}, and I_{am} are the integral intensities of the diffraction reflections of *Mt*, Bent crystalline phase and PDMS amorphous phase, respectively.

The piezoelectric measurement results are consistent with the X-ray diffraction measurements (Figs. 11 and 12), which show that the crystalline order and crystalline fraction volume (CVF_{Mt}) of the PDMS-Bent composite films increases with the increasing percentage of Bent, *Mt* crystalline phase being the predominant component in diffractograms. Logically, the crystalline volume fraction of *Mt* increases with increasing of Bent content and reaches a value of about 12.2% for 100 pph Bent load. The gentle incorporation of Bent into the silicone matrix by simply mixing in the solution ensures unaltered preservation of Bent crystallinity, which is reflected in the piezoelectric-like response of the material obtained on its basis. There is a strong correlation between crystalline volume fraction of *Mt* (CVF_{Mt}), pseudo-piezoelectric performance (apparent d_{33}) and breakdown field of *Cn* composite. The increase of CVF_{Mt} with Bent content is accompanied by a similar increase of the piezoelectric-like response and a somewhat mirror-like decrease in breakdown field (Fig. 12, inset).

Typically, the piezoelectric response depends inversely on the elastic modulus (*Y*) of the polymer matrix [51,55]. In this case, although the Young modulus increases as the Bent concentration increases, the apparent d_{33} coefficient is also directly proportional to the Bent concentration. It seems that the effect of increased Young modulus is counterbalanced by the electrostriction, which is generally defined as a quadratic coupling between the strain and the polarization. Since the polarization is strongly related to the crystalline volume fraction of *Mt* (CVF_{Mt}), we can conclude that the CVF_{Mt} is the

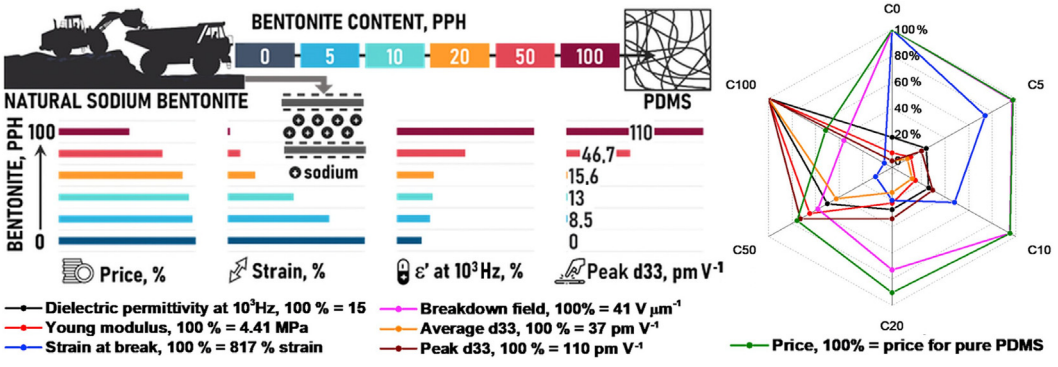

Fig. 13 – An overview of prepared composites and their performance in terms of dielectric, mechanical, and piezo-like properties, as well as cost, in dependence on bentonite loading (left), including spider chart representation (right).

main factor which influences the piezoelectric-like performances of *Cn* composite.

It should be noted that the PDMS-Bent polymer composite samples stored in laboratory conditions in polycarbonate box, show almost the same piezoresponse-like effect after eight months from the processing date. By associating Bent electrets with an electrostrictive elastic polymer opens up new perspectives in getting autonomous micro-generators, electromechanical transducers and energy harvesters [40,56,62]. Also, the ability to endure large strains makes the hybridization of Bent electrets and electrostrictive polymers perfect candidates for smart textiles and tactile sensors.

To have a better view of the influence of Bent on the silicone matrix, a centralization of the main results was made and a spider chart was plotted (Fig. 13). Comparing prices for PDMS and Bent from the same store, it was found that Bent is over 33 times cheaper than PDMS. Besides, the cost price can be reduced up to over 40% by using the Bent as filler, and the mechanical, thermal and dielectric properties are also changed. Using of Bent to reduce the price without significantly modifying the properties of the silicone matrix is possible until 10 pph loading of the filler. With increasing the Bent content, the properties of the silicone matrix change greatly and the piezoelectric-like response is increased.

The results show that improvements of some characteristics (i.e., dielectric and piezo-like response) are obtained to the detriment of others (mechanical elongation or dielectric strength), and this would limit the application of these materials to electromechanical devices where both dielectric and mechanical properties are of interest. However, the use of the piezoelectric-like response is conditioned only by the physical integrity of the material, which is appropriate in all cases.

4. Conclusions

The incorporation of bentonite into PDMS in increasing amounts leads mainly to the improvement of dielectric permittivity and piezoresponse-like performances although to the detriment of the elasticity and the dielectric strength. In addition, the resulting material has a lower cost. It has been found that the Young modulus increases up to 61 times, while break elongation decreases 70 times for composite with Bent content of 100 pph, as compared to pure PDMS. Dielectric permittivity, at 10^3 Hz, increases of about five times at this Bent content, but unfortunately dielectric losses also increase. Instead, Bent filler induces the piezoelectric-like response of the silicone composites with average apparent d_{33} piezoelectric constant, as estimated by PFM, up to 37 pm V^{-1} for the sample with 100 pph Bent. This value, confirmed also by direct piezoelectric measurements, is comparable to that of the traditional piezoelectric ceramics and ferroelectric polymers. It is worthwhile to say that under the same experimental conditions, a PDMS reference gave practically no piezoelectric response. The crystalline volume fraction of *Mt* is considered the main factor that influences the piezoelectric-like performance of PDMS-Bent composite. The gentle incorporation of Bent into the silicone matrix by simply mixing in the solution ensures unaltered preservation of Bent crystallinity. PDMS-Bent composites are flexible under deformation, are cost-effective in preparation and shows high pseudo-piezoelectric response, all of which making composite film a very attractive candidate material for flexible electronics and electromechanical transducers.

Author contributions

Mihail Iacob (conceptualization, data curation, formal analysis, writing-original draft), Vasile Tiron (conceptualization, investigation, writing-original draft, writing-review & editing), George Stiubianu (methodology, investigation), Mihaela Dascalu (investigation), Leonor Hernandez (methodology), Cristian Dragos Varganici (investigation), Codrin Tugui (methodology, data curation, validation), Maria Cazacu (conceptualization, project administration, writing-original draft, writing-review & editing).

Declaration of Competing Interest

The authors declare that they have no known competing financial interests or personal relationships that could have appeared to influence the work reported in this paper.

Acknowledgements

This work was supported by a grant of the Romanian Ministry of Research, Innovation and Digitization, CNCS/CCCDI-UEFISCDI, project number PN-III-P2-2.1-PED-2019-3652, within PNCDI III (Contract 320/2020, 3DETSi) and COST Action CA15119.

Appendix A. Supplementary data

Supplementary data to this article can be found online at https://doi.org/10.1016/j.jmrt.2021.12.125.

REFERENCES

[1] Nguyen Q, Baird D. Preparation of polymer–clay nanocomposites and their properties. Adv Polym Technol 2006;25:270–85. https://doi.org/10.1002/adv.20079.
[2] Ma P, Chen H, Zhang Q, Wang J, Xiang L. Preparation of hierarchical CaSO4 whisker and its reinforcing effect on PVC composites. J Nanomater 2018;2018:1–7. https://doi.org/10.1155/2018/7803854.
[3] Gao Y, Liu L, Zhang Z. Mechanical performance of nano-CaCO3 filled polystyrene composites. Acta Mech Solida Sin 2009;22:555–62. https://doi.org/10.1016/S0894-9166(09)60386-4.
[4] Lapcik L, Jindrova P, Lapcikova B, Tamblyn R, Greenwood R, Rowson N. Effect of the talc filler content on the mechanical properties of polypropylene composites. J Appl Polym Sci 2008;110:2742–7. https://doi.org/10.1002/app.28797.
[5] Bataille P, Boisse S, Schreiber H. Mica as filler for PVC compounds: effects of particle size and surface treatment. J. VINYL Technol. 1984;6:147–51.
[6] Bala P, Samantaray BK, Srivastava SK, Nando GB. Organomodified montmorillonite as filler in natural and

synthetic rubber. J Appl Polym Sci 2004;92:3583–92. https://doi.org/10.1002/app.20401.
[7] Kim JH, Hwang JY, Hwang HR, Kim HS, Lee JH, Seo JW, et al. Simple and cost-effective method of highly conductive and elastic carbon nanotube/polydimethylsiloxane composite for wearable electronics. Sci Rep 2018;8:1–11. https://doi.org/10.1038/s41598-017-18209-w.
[8] Mao Y, Wen S, Chen Y, Zhang F, Panine P, Chan TW, et al. High performance graphene oxide based rubber composites. Sci Rep 2013;3:1–7. https://doi.org/10.1038/srep02508.
[9] Iacob M, Airinei A, Asandulesa M, Dascalu M, Tudorachi N, Hernandez L, et al. Silicone elastomers filled with rare earth oxides. Mater Res Express 2020;7:035703. https://doi.org/10.1088/2053-1591/ab7a5e.
[10] Kurian AS, Mohan VB, Souri H, Leng J, Bhattacharyya D. Multifunctional flexible and stretchable graphite-silicone rubber composites. J Mater Res Technol 2020;9(6):15621–30. https://doi.org/10.1016/j.jmrt.2020.11.021.
[11] Rothon R. Fillers for polymer applications. Gewerbestrasse: Springer International Publishing; 2017. https://doi.org/10.1007/978-3-319-28117-9.
[12] Mat NSC, Ismail H, Othman N. Curing characteristics and tear properties of bentonite filled ethylene propylene diene (EPDM) rubber composites. Procedia Chem 2016;19:394–400. https://doi.org/10.1016/j.proche.2016.03.029.
[13] Bhattacharya M. Polymer nanocomposites-A comparison between carbon nanotubes, graphene, and clay as nanofillers. Materials (Basel) 2016;9:1–35. https://doi.org/10.3390/ma9040262.
[14] Uğur Ş, Yargi Ö, Elaissari A, Pekcan Ö. Oxygen diffusion into polymer-clay composite films as a function of clay content and temperature. Macromol Symp 2009;281:168–73. https://doi.org/10.1002/masy.200950722.
[15] Meng N, Zhou NL. Synthesis and properties of PDMS/montmorillonite-cetyltrimethylammonium bromide-heparin films. Carbohydr Polym 2014;105:70–4. https://doi.org/10.1016/j.carbpol.2014.01.052.
[16] Lebaron PC, Wang Z, Pinnavaia TJ. Polymer-layered silicate nanocomposites: an overview. Appl Clay Sci 1999;15:11–29. https://doi.org/10.1016/S0169-1317(99)00017-4.
[17] Gao F. Clay/polymer composites: the story. Mater Today 2004;7:50–5. https://doi.org/10.1016/S1369-7021(04)00509-7.
[18] Shit SC, Shah P. A review on silicone rubber. Natl Acad Sci Lett 2013;36:355–65. https://doi.org/10.1007/s40009-013-0150-2.
[19] Ştiubianu G, Soroceanu A, Varganici CD, Tugui C, Cazacu M. Dielectric elastomers based on silicones filled with transitional metal complexes. Compos B Eng 2016;93:236–43. https://doi.org/10.1016/j.compositesb.2016.03.005.
[20] Iacob M, Bele A, Patras X, Pasca S, Butnaru M, Alexandru M, et al. Preparation of electromechanically active silicone composites and some evaluations of their suitability for biomedical applications. Mater Sci Eng C 2014;43:392–402. https://doi.org/10.1016/j.msec.2014.07.031.
[21] Bele A, Tugui C, Sacarescu L, Iacob M, Stiubianu G, Dascalu M, et al. Ceramic nanotubes-based elastomer composites for applications in electromechanical transducers. Mater Des 2018;141:120–31. https://doi.org/10.1016/j.matdes.2017.12.039.
[22] Iacob M, Tugui C, Tiron V, Bele A, Vlad S, Vasiliu T, et al. Iron oxide nanoparticles as dielectric and piezoelectric enhancers for silicone elastomers. Smart Mater Struct 2017;26. https://doi.org/10.1088/1361-665X/aa867c.
[23] Racles C, Musteata VE, Bele A, Dascalu M, Tugui C, Matricala AL. Highly stretchable composites fROU PDMS and polyazomethine fine particles. RSC Adv 2015;5:102599–609. https://doi.org/10.1039/c5ra12297j.
[24] Iacob M, Stiubianu G, Tugui C, Ursu L, Ignat M, Turta C, et al. Goethite nanorods as a cheap and effective filler for siloxane nanocomposite elastomers. RSC Adv 2015;5:45439–45. https://doi.org/10.1039/c5ra03765d.
[25] Stiubianu G, Dumitriu AMC, Varganici CD, Tugui C, Iacob M, Bele A, et al. Changes induced in the properties of dielectric silicone elastomers by the incorporation of transition metal complexes. High Perform Polym 2016;28:915–26. https://doi.org/10.1177/0954008315610393.
[26] Bele A, Tugui C, Asandulesa M, Ionita D, Vasiliu L, Stiubianu G, et al. Conductive stretchable composites properly engineered to develop highly compliant electrodes for dielectric elastomer actuators. Smart Mater Struct 2018;27:105005. https://doi.org/10.1088/1361-665X/aad977.
[27] Cazacu M, Marcu M. Silicone rubbers. ix. contributions to polydimethylsiloxane-α,ω-diols synthesis by heterogeneous catalysis. J Macromol Sci Part A 1995;32:1019–29. https://doi.org/10.1080/10601329508019142.
[28] Tugui C, Ursu C, Zaltariov MF, Aflori M, Mičušík M, Omastová M, et al. Silver thin films generated by Pulsed Laser Deposition on plasma-treated surface of silicones to get dielectric elastomer transducers. Surf Coating Technol 2019;358:282–92. https://doi.org/10.1016/j.surfcoat.2018.11.009.
[29] Alexe M, Gruverman A. Nanoscale characterisation of ferroelectric materials. Scanning probe microscopy approach. Berlin: Springer Berlin Heidelberg; 2001. https://doi.org/10.1007/978-3-662-08901-9.
[30] Balke N, Bdikin I, Kalinin SV, Kholkin AL. Electromechanical imaging and spectroscopy of ferroelectric and piezoelectric materials: state of the art and prospects for the future. J Am Ceram Soc 2009;92:1629–47. https://doi.org/10.1111/j.1551-2916.2009.03240.x.
[31] Soergel E. Piezoresponse force microscopy (PFM). J Phys D Appl Phys 2011;44:464003. https://doi.org/10.1088/0022-3727/44/46/464003.
[32] Gomez A, Gich M, Carretero-Genevrier A, Puig T, Obradors X. Piezo-generated charge mapping revealed through direct piezoelectric force microscopy. Nat Commun 2017;8:1–10. https://doi.org/10.1038/s41467-017-01361-2.
[33] Harnagea C, Pignolet A, Alexe M, Hesse D. Piezoresponse scanning force microscopy: what quantitative information can we really get out of piezoresponse measurements on ferroelectric thin films. Integr. Ferroelectr. Int. J. 2001;38:23–9. https://doi.org/10.1080/10584580108016914.
[34] Miao H, Tan C, Zhou X, Wei X, Li F. More ferroelectrics discovered by switching spectroscopy piezoresponse force microscopy? Epl 2014;108:27010. https://doi.org/10.1209/0295-5075/108/27010.
[35] Seol D, Kim B, Kim Y. Non-piezoelectric effects in piezoresponse force microscopy. Curr Appl Phys 2017;17:661–74. https://doi.org/10.1016/j.cap.2016.12.012.
[36] Christman JA, Woolcott RR, Kingon AI, Nemanich RJ. Piezoelectric measurements with atomic force microscopy. Appl Phys Lett 1998;73:3851–3. https://doi.org/10.1063/1.122914.
[37] Gomez A, Puig T, Obradors X. Diminish electrostatic in piezoresponse force microscopy through longer or ultra-stiff tips. Appl Surf Sci 2018;439:577–82. https://doi.org/10.1016/j.apsusc.2018.01.080.
[38] Macdonald GA, Delrio FW, Killgore JP. Higher-eigenmode piezoresponse force microscopy: a path towards increased sensitivity and the elimination of electrostatic artifacts. Nano Futur 2018;2:015005. https://doi.org/10.1088/2399-1984/aab2bc.
[39] Racles C, Ursu C, Dascalu M, Asandulesa M, Tiron V, Bele A, et al. Multi-stimuli responsive free-standing films of DR1-

grafted silicones. Chem Eng J 2020;401:126087. https://doi.org/10.1016/j.cej.2020.126087.
[40] Tugui C, Bele A, Tiron V, Hamciuc E, Varganici CD, Cazacu M. Dielectric elastomers with dual piezo-electrostatic response optimized through chemical design for electromechanical transducers. J Mater Chem C 2017;5:824–34. https://doi.org/10.1039/c6tc05193f.
[41] Zhirong L, Azhar Uddin M, Zhanxue S. FT-IR and XRD analysis of natural Na-bentonite and Cu(II)-loaded Na-bentonite. Spectrochim Acta - Part A Mol Biomol Spectrosc 2011;79:1013–6. https://doi.org/10.1016/j.saa.2011.04.013.
[42] Hayati-Ashtiani M. Use of FTIR spectroscopy in the characterization of natural and treated nanostructured bentonites (montmorillonites), Part. Sci. Technol. An Int. J. 2012;30:553–64. https://doi.org/10.1080/02726351.2011.615895.
[43] Thomas TH, Kendrick TC. Thermal analysis of polydimethylsiloxanes. I. Thermal degradation in controlled atmospheres. J Polym Sci 2 Polym Phys 1969;7:537–49. https://doi.org/10.1002/pol.1969.160070308.
[44] Thomas TH, Kendrick TC. Thermal analysis of polysiloxanes. II.Thermal vacuum degradation of polysiloxanes with different substituents on silicon and in the main siloxane chain. J Polym Sci 2 Polym Phys 1970;8:1823–30.
[45] Ben Ishai P, Talary MS, Caduff A, Levy E, Feldman Y. Electrode polarization in dielectric measurements: a review. Meas Sci Technol 2013;24:102001. https://doi.org/10.1088/0957-0233/24/10/102001.
[46] Tugui C, Stiubianu GT, Serbulea MS, Cazacu M. Silicone dielectric elastomers optimized by crosslinking pattern-a simple approach to high-performance actuators. Polym Chem 2020;11:3271–84. https://doi.org/10.1039/d0py00223b.
[47] Song H. Fabrication and characterisation of electrospun polyvinylidene fluoride (PVDF) nanocomposites for energy harvesting applications. Brunel University London; 2016.
[48] Gheorghiu F, Stanculescu R, Curecheriu L, Brunengo E, Stagnaro P, Tiron V, et al. PVDF–ferrite composites with dual magneto-piezoelectric response for flexible electronics applications: synthesis and functional properties. J Mater Sci 2020;55:3926–39. https://doi.org/10.1007/s10853-019-04279-w.
[49] Neumayer SM, Saremi S, Martin LW, Collins L, Tselev A, Jesse S, et al. Piezoresponse amplitude and phase quantified for electromechanical characterization. J Appl Phys 2020;128:171105. https://doi.org/10.1063/5.0011631.
[50] Collins L, Liu Y, Ovchinnikova OS, Proksch R. Quantitative electromechanical atomic force microscopy. ACS Nano 2019;13:8055–66. https://doi.org/10.1021/acsnano.9b02883.
[51] Wan Y, Xie L, Zhong Z. Micromechanical prediction of the effective electromechanical properties of cellular ferroelectrets. J Appl Phys 2010;108:054101. https://doi.org/10.1063/1.3481435.
[52] Mellinger A. Dielectric resonance spectroscopy: a versatile tool in the quest for better piezoelectric polymers. IEEE Trans Dielectr Electr Insul 2003;10(50):842–61.
[53] Belhora F, Cottinet PJ, Guyomar D, Lebrun L, Hajjaji A, Mazroui M, et al. Hybridization of electrostrictive polymers and electrets for mechanical energy harvesting. Sensors Actuators, A Phys. 2012;183:50–6. https://doi.org/10.1016/j.sna.2012.05.044.
[54] Luckham PF, Rossi S. Colloidal and rheological properties of bentonite suspensions. Adv Colloid Interface Sci 1999;82:43–92. https://doi.org/10.1016/S0001-8686(99)00005-6.
[55] Hillenbrand J, Sessler GM. Piezoelectricity in cellular electret films. IEEE Trans Dielectr Electr Insul 2000;7:537–42. https://doi.org/10.1109/94.868074.Z.Wang.
[56] Ramadan KS, Sameoto D, Evoy S. A review of piezoelectric polymers as functional materials for electromechanical transducers. Smart Mater Struct 2014;23:033001.
[57] Prodromakis T, Papavassiliou C. Engineering the maxwell–wagner polarization effect. Appl Surf Sci 2009;255:6989–94.
[58] Li C, Chen G, Qiu X, Lou Q, Gao X. A direct proof for Maxwell–Wagner effect of heterogeneous interface. AIP Adv 2021;11:065227.
[59] Qiao B, Wang X, Tan S, Zhu W, Zhang Z. Synergistic effects of Maxwell stress and electrostriction in electromechanical properties of poly(vinylidene fluoride)-based ferroelectric polymers. Macromolecules 2019;52:9000–11.
[60] Sessler GM. Electrets. Second Enlarged Edition. Berlin, Heidelberg: Springer- Berlag; 1987.
[61] Yang J, Han YM, Zhang DX, Fu B, Ye RC. Magnetostriction and effective magnetic anisotropy of Co-contained Finemet nanocrystalline alloys. J Appl Phys 2010;107:1–4. https://doi.org/10.1063/1.3340514.
[62] Racles C, Dascalu M, Bele A, Tiron V, Asandulesa M, Tugui C, et al. All-silicone elastic composites with counter-intuitive piezoelectric response, designed for electromechanical applications. J Mater Chem C 2017;5:6997–7010. https://doi.org/10.1039/c7tc02201h.